Spectral–Spatial Classification of Hyperspectral Imagery Based on Partitional Clustering Techniques

Yuliya Tarabalka, *Student Member, IEEE*, Jón Atli Benediktsson, *Fellow, IEEE*, and Jocelyn Chanussot, *Senior Member, IEEE*

***Abstract*—A new spectral–spatial classification scheme for hyperspectral images is proposed. The method combines the results of a pixel wise support vector machine classification and the segmentation map obtained by partitional clustering using majority voting. The ISODATA algorithm and Gaussian mixture resolving techniques are used for image clustering. Experimental results are presented for two hyperspectral airborne images. The developed classification scheme improves the classification accuracies and provides classification maps with more homogeneous regions, when compared to pixel wise classification. The proposed method performs particularly well for classification of images with large spatial structures and when different classes have dissimilar spectral responses and a comparable number of pixels.**

***Index Terms*—Clustering, hyperspectral images, majority vote, segmentation, spectral–spatial classification.**

I. Introduction

THE ACCURATE classification of remote sensing images is an important task for many practical applications, such as precision agriculture, monitoring and management of the environment, and security and defense issues. The advent and growing availability of hyperspectral imagery, which records hundreds of spectral bands, has opened new possibilities in image analysis and classification. Examples of hyperspectral imaging systems are Airborne Visible/Infrared Imaging Spectrometer (AVIRIS) [1], HYDICE [2], ARCHER [3], HyMap [4], and Hyperion [5]. They cover a range of 126–512 spectral channels, with the spatial resolution of 3–30 m per pixel. Thus, every pixel in a hyperspectral image contains values that correspond to the detailed spectrum of reflected light [6]. This rich spectral information in every spatial location increases the capability to distinguish different physical materials and objects, leading to the potential of a more accurate image classification.

Manuscript received October 3, 2008; revised December 16, 2008. First published April 24, 2009; current version published July 23, 2009. This work was supported in part by the Marie Curie Research Training Network "HYPER-I-NET."

Y. Tarabalka is with the Faculty of Electrical and Computer Engineering, University of Iceland, 107 Reykjavik, Iceland and also with the GIPSA-Lab-Grenoble Institute of Technology, Domaine Universitaire, 38402 Saint-Martin-d'Hères Cedex, France (e-mail: yuliya.tarabalka@hyperinet.eu).

J. A. Benediktsson is with the Faculty of Electrical and Computer Engineering, University of Iceland, 107 Reykjavik, Iceland (e-mail: benedikt@hi.is).

J. Chanussot is with GIPSA-Lab-Grenoble Institute of Technology, Domaine Universitaire, 38402 Saint-Martin-d'Hères Cedex, France (e-mail: jocelyn.chanussot@lis.inpg.fr).

Color versions of one or more of the figures in this paper are available online at http://ieeexplore.ieee.org.

Digital Object Identifier 10.1109/TGRS.2009.2016214

An extensive literature is available on the classification of hyperspectral images where a wide range of pixel-level processing techniques is proposed, i.e., techniques that assign each pixel to one of the classes based on its spectral values. Maximum-likelihood or Bayesian estimation methods [7], decision trees [8], [9], neural networks [10]–[12], genetic algorithms [13], and kernel-based techniques [14], [15] have been investigated for this purpose. In particular, support vector machines (SVMs) have shown a good performance for classifying high-dimensional data when a limited number of training samples are available [14], [16], [17].

To improve classification results, the contextual information should be considered for incorporation into the classifiers. Spectral–spatial classification aims at assigning each image pixel to one class using a feature vector based on the following: 1) its own spectral value (the spectral information) and 2) information extracted from its neighborhood (referred to as the spatial information in the following). One of the approaches of spectral–spatial classification consists in including the information from the closest neighborhood to classify each pixel. These fixed-window-based methods that use morphological filtering [15], morphological leveling [18], [19], or Markov random fields [20] have shown improvements in classification accuracies compared to the pixel wise methods, when applied to hyperspectral images. However, the use of these methods raises the problem of scale selection, particularly when small or complex structures are present in the image.

Another approach to include spatial information in classification consists in performing image segmentation. *Segmentation* can be defined as an exhaustive partitioning of the input image into regions, each of which is considered to be homogeneous with respect to some criterion of interest (homogeneity criterion, e.g., intensity or texture) [21]. These regions form a segmentation map that can be used as spatial structures for a spectral–spatial classification.

In this paper, we propose a new *spectral–spatial classification scheme* for hyperspectral data. The proposed method combines the results of a pixel wise spectral classification and a segmentation map, aiming to improve classification accuracies, when compared to pixel wise classification only.

Fu and Mui [22] identified three classes of image segmentation techniques: *edge-based*, *region-based*, and *characteristic feature thresholding* or *clustering*. Lambert and Macaire [23] have split the last class into two: *histogram-based* and *cluster-based* methods. *Edge-based* techniques search for discontinuities in the image, while *region-based* techniques search for similarities between image regions. Methods from these two

classes operate in the spatial domain. Their adaptation to the multidimensional images is a challenging task.

The other two, *histogram-based* and *cluster-based* techniques, work in the spectral domain. They search for similarities between image pixels and clusters of pixels, not taking into consideration the spatial location of these pixels. The *histogram-based* methods relate the modes of a spectral histogram to homogeneous regions in the image [24], [25]. With a high dimensionality, these methods become memory consuming and produce less accurate results. The *cluster-based* segmentation techniques aim at finding distinct structures in the spectral feature space. Thus, *clustering* is an exhaustive partitioning of a set of pixels from the input image into homogeneous groups of pixels. In this paper, the *cluster-based* segmentation of hyperspectral images will be explored.

A taxonomy and survey of clustering techniques can be found in [26]. Two principal groups of clustering methods can be distinguished: hierarchical and partitional approaches. Hierarchical methods usually produce a dendrogram, where at the lowest level, each cluster contains only one pixel (i.e., each pixel forms a cluster), and with the increase of levels, the most similar clusters are merged (and the number of clusters decreases). Then, the result with the desired number of clusters can be chosen. Lee and Crawford [27] have applied the hierarchical clustering approach for unsupervised classification of hyperspectral images. Although hierarchical clustering is a versatile technique for image segmentation that can produce a series of segmentation results, it requires a lot of computational time. Its application to high-dimensional data leads to significant time and memory requirements, and it becomes more difficult to cope with large dendrograms.

In this paper, the use of partitional clustering for hyperspectral image segmentation is investigated. Two algorithms are considered for this purpose: ISODATA (squared-error clustering method) [28] and expectation maximization (EM) for the Gaussian mixture resolving [29]. These algorithms produce a single partition of the data, and the number of desired clusters must be chosen. The other problem accompanying the use of these techniques is that the clustering results depend on the initialization (it will be discussed in the next sections). However, the computational complexity of these algorithms is lower than that in the case of hierarchical clustering. Moreover, efficient implementations are possible. Venkateswarlu and Raju [30] proposed an algorithm to speed up the ISODATA algorithm. Tarabalka *et al.* [31] have shown that the parallel implementation of the EM algorithm on the graphical processing unit is feasible and efficient.

The results of hyperspectral image segmentation are further incorporated into a spectral–spatial classifier. The SVM classifier is used in the proposed method. In previous studies, the integration of spectral and spatial information into classifier with the use of SVM was achieved in different ways: Within the framework of composite kernels, spectral and contextual information was combined using composite kernels and then each pixel was classified [19], [32]–[35]. Van der Linden *et al.* [36] used another approach which consisted of computing a vector mean for each region (such that the value in each spectral channel represented the average spectral information of the pixels in this region in the respective channel) and then using this vector as a feature vector to classify each region by an SVM classifier. The use of composite kernels led to the improvement of the classification accuracies when compared to an SVM classification using spectral information only; however, the approach of classifying regions using their vector means did not show any improvement over results obtained by using only a spectral-based pixel wise SVM classification.

Here, we propose a new spectral–spatial classification scheme, where pixel wise SVM classification and segmentation by clustering are performed independently, and then, the results are combined using the *majority vote* approach [37]. Thus, the segmentation defines an *adaptive neighborhood* for each pixel. These neighborhoods are then used for the contextual regularization following a spectral pixel wise classification. Finally, a spatial postregularization (PR) of the classification map is performed.

Although the proposed scheme has been designed for hyperspectral images, the method is general and can be applied for other types of data as well.

Two hyperspectral airborne images were used to demonstrate experimental results: a 103-band Reflective Optics System Imaging Spectrometer (ROSIS) image of the University of Pavia, Italy, and a 220-band AVIRIS image taken over the Northwestern Indiana's Indian Pine site [38].

The outline of this paper is as follows. In Section II, segmentation of hyperspectral data using partitional clustering techniques is discussed. Section III describes the proposed spectral–spatial classification scheme. Experimental results are discussed in Section IV. Finally, conclusions are drawn in Section V.

II. Segmentation of Hyperspectral Data by Partitional Clustering

In this section, we first describe two techniques for partitional clustering of hyperspectral data. Then, the segmentation scheme based on the partitional clustering is presented.

A. Clustering by ISODATA and EM

As was mentioned earlier, clustering implies a grouping of pixels in the spectral space. Let us consider the input hyperspectral image as a set of n pixel vectors $\mathbf{X} = \{\mathbf{x}_j \in \mathbf{R}^B, j = 1, 2, \ldots, n\}$, where B is the number of spectral bands. Each pixel in the image is characterized by its spatial location (coordinates) and vector of spectral values. The information about spatial positions of pixels is not used in the clustering algorithms. However, it is taken into consideration during the second stage of the segmentation procedure (as will be explained in the next section).

The three principal stages of the clustering technique are as follows.

1) *Feature selection/extraction*: *Feature selection* consists in identifying a subset of the original features. *Feature extraction* consists in applying one or more transformations of the input features to produce new salient features. Either or both of these techniques can be applied to obtain the most effective set of features to be used in clustering.

As a pixel vector from hyperspectral image contains hundreds of spectral values, feature extraction/selection is often a required step to reduce the dimensionality of the clustering/classification problem. The most common transformations applied to these images are principal component analysis (PCA) [39], minimum noise fraction [40], and independent component analysis (ICA) [41]–[43]. Furthermore, when describing clustering algorithms, we consider, for the sake of simplicity, that $\mathbf{X}$ is already a set of feature vectors (we also call it a *set of patterns*).

2) *Similarity measure*: Clustering aims at grouping pixels, so that pixels belonging to the same cluster are spectrally similar. To quantify this relationship, a similarity measure must be chosen. Proximity between pixels is usually measured by a distance function defined on pairs of spectral values. A simple distance measure like the Euclidean distance is often used to measure similarity between vectors. For some cases, other measures can be more relevant. Description of various distance measures can be found in [26], [44], and [45].

3) *Grouping*: In this step, pixels are grouped into clusters. Partitional clustering algorithms identify the partition that optimizes a clustering criterion (deducted from the similarity measure step).

Both ISODATA and EM are iterative optimization techniques. Thus, on each iteration i, a partition $\mathbf{Q}_1^i, \mathbf{Q}_2^i, \ldots, \mathbf{Q}_C^i$ of the set $\mathbf{X}$ into C clusters is computed, so that $\mathbf{Q}_c^i = \{\mathbf{x}_{j,c}^i \in \mathbf{R}^B, j = 1, 2, \ldots, m_c^i\}$ contains the pixels belonging to the component c on the iteration i, where m_c^i is the number of pixels in $\mathbf{Q}_c^i$.

1) ISODATA Algorithm: As described in [26], the simplest and most frequently used criterion in partitional clustering is the squared-error criterion, which is the most suitable in the case of isolated and compact clusters. The squared error for a clustering Υ of a set $\mathbf{X}$ into C clusters is defined as

$$e^2(\mathbf{X}, \Upsilon) = \sum_{c=1}^{C} \sum_{j=1}^{m_c} \|\mathbf{x}_{j,c} - \boldsymbol{\mu}_c\|^2 \tag{1}$$

where $\boldsymbol{\mu}_c$ is the centroid of the cluster c.

ISODATA clustering is a well-known algorithm introduced by Ball and Hall [28] which uses the squared-error criterion. It starts with a random initial partition of the pixel vectors into candidate clusters and then reassigns these vectors to clusters in such a way that the squared error (1) is reduced at each iteration, until a convergence criterion is achieved [39]. The algorithm permits splitting, merging, and deleting of clusters at each iteration in order to produce more accurate results and to mitigate dependence of results on the initialization.

The ISODATA algorithm is implemented in the ENVI software [46], where its application for hyperspectral images is straightforward. A vector of spectral values can be used as a feature vector for every pixel. When we have a reference map for the images, we can define a *minimum* number of clusters $C_{\min}$ equal to the number of classes in the reference map and choose a *maximum* number of clusters $C_{\max}$ superior to this value.

Several methods have used the ISODATA algorithm in remote sensing analysis. Kamagata *et al.* [47] applied the algorithm to classify multispectral IKONOS data. It was also used by Liew *et al.* [48] to classify hyperspectral Hyperion images.

2) EM Algorithm: While ISODATA is a deterministic clustering approach, the EM algorithm belongs to the group of statistical algorithms that assume a statistical model that characterizes the data.

The underlying assumption for the mixture resolving approach to cluster analysis (that includes the EM algorithm) is that the patterns are drawn from one or several distributions. The objective is to identify the parameters of each distribution. Most often, the individual components of the mixture density are assumed to be Gaussian. In this case, the parameters of a Gaussian mixture model have to be estimated.

The EM algorithm was proposed by Dempster *et al.* [29] to obtain iteratively a maximum likelihood estimate of the parameters of component densities from the patterns.

To cluster a hyperspectral image by the EM technique, we assume that pixels belonging to the same cluster are drawn from a multivariate Gaussian probability distribution. Each image pixel can be statistically modeled by the following probability density function:

$$p(\mathbf{x}) = \sum_{c=1}^{C} \omega_c \phi_c(\mathbf{x}; \boldsymbol{\mu}_c, \boldsymbol{\Sigma}_c) \tag{2}$$

where $\omega_c \in [0, 1]$ is the mixing proportion (weight) of cluster c with $\sum_{c=1}^{C} \omega_c = 1$ and $\phi(\boldsymbol{\mu}, \boldsymbol{\Sigma})$ is the multivariate Gaussian density with mean $\boldsymbol{\mu}$ and covariance matrix $\boldsymbol{\Sigma}$

$$\phi_c(\mathbf{x}; \boldsymbol{\mu}_c, \boldsymbol{\Sigma}_c) = \frac{1}{(2\pi)^{B/2}} \frac{1}{|\boldsymbol{\Sigma}_c|^{1/2}} \times \exp\left\{-\frac{1}{2}(\mathbf{x} - \boldsymbol{\mu}_c)^{\mathrm{T}} \boldsymbol{\Sigma}_c^{-1} (\mathbf{x} - \boldsymbol{\mu}_c)\right\}. \tag{3}$$

The parameters of the distributions $\boldsymbol{\psi} = \{C, \omega_c, \boldsymbol{\mu}_c, \boldsymbol{\Sigma}_c; c = 1, 2, \ldots, C\}$ are estimated by an iterative method similar to the classification EM algorithm [49], as outlined in Algorithm 1 [31]. During the procedure of parameter estimation, pixels are assigned to the C clusters. Therefore, when the algorithm converges, the partitioning of the set of pixel vectors into C clusters is obtained.

Algorithm 1 EM clustering

Require:

- a set of n feature vectors (patterns) $\mathbf{X}$
- an upper bound $C_{\max}$ on the number of clusters

Initialization (Iteration 0):

Let $C = C_{\max}$. Determine the first partition $\mathbf{Q}_c^0$, $c = 1, 2, \ldots, C$ of $\mathbf{X}$:

1. Choose randomly C patterns from the set $\mathbf{X}$ to serve as cluster centers.

2. Assign the remaining patterns to the clusters on the basis of the nearest Euclidean distance to the cluster center.

For every iteration $i > 0$ (I iterations in total):

Parameter estimation step:

Estimate $\boldsymbol{\mu}_c^i$, $\boldsymbol{\Sigma}_c^i$, and ω_c^i for $c = 1, 2, \ldots, C$ using the component-wise Maximum Likelihood estimates

$$\boldsymbol{\mu}_c^i = \frac{1}{m_c^{i-1}} \sum_{j=1}^{m_c^{i-1}} \mathbf{x}_{j,c}^{i-1} \tag{4}$$

$$\boldsymbol{\Sigma}_c^i = \frac{1}{m_c^{i-1}} \sum_{j=1}^{m_c^{i-1}} \left(\mathbf{x}_{j,c}^{i-1} - \boldsymbol{\mu}_c^i\right)\left(\mathbf{x}_{j,c}^{i-1} - \boldsymbol{\mu}_c^i\right)^{\mathrm{T}} \tag{5}$$

$$\omega_c^i = \frac{m_c^{i-1}}{n}. \tag{6}$$

Cluster assignment step:

1. Assign each pattern in $\mathbf{X}$ to one of the clusters according to the maximum *a posteriori* probability criteria

$$\mathbf{x}_j \in \mathbf{Q}_c^i : \Pr(c|\mathbf{x}_j) = \max_l \Pr(l|\mathbf{x}_j) \tag{7}$$

where

$$\Pr(c|\mathbf{x}_j) = \frac{\omega_c^i \phi_c\left(\mathbf{x}_j; \boldsymbol{\mu}_c^i, \boldsymbol{\Sigma}_c^i\right)}{\sum_{c=1}^{C} \omega_c^i \phi_c\left(\mathbf{x}_j; \boldsymbol{\mu}_c^i, \boldsymbol{\Sigma}_c^i\right)}. \tag{8}$$

2. Eliminate cluster c if m_c^i is less than the dimensionality of patterns, $c = 1, 2, \ldots, C$. The patterns that belonged to the deleted clusters will be reassigned to the other clusters in the next iteration.

3. If the convergence criterion is not achieved, return to the parameter estimation step.

The total number of parameters to be estimated is $P = (B(B+1)/2 + B + 1)C + 1$, where B is a dimensionality of feature vectors. If the value of B is large, P may be quite a large number. This may cause the problem of the covariance matrix singularity or inaccurate parameter estimation results. To avoid these problems, we reduce the spectral dimension of pixel vectors in hyperspectral data by averaging every AW neighboring bands, so that

$$x_{j,b}^{\mathrm{av}} = \frac{\sum_{i=1}^{AW} x_{j,[(b-1)AW+i]}}{AW} \tag{9}$$

where $x_{j,i}$ is a value of pixel x_j in the input band i and $x_{j,b}^{\mathrm{av}}$ is a value of pixel x_j in the output band b; $j = 1, \ldots, n$, $b = 1, \ldots, B_{\mathrm{av}}$, where $B_{\mathrm{av}} = n/AW$.

This is a simple way of feature extraction. In previous studies, the feature extraction methods appropriate for hyperspectral image analysis, such as the PCA, the ICA, the ISOMAP and clustering-based band selection were considered [39], [42], [50], [51]. The research question to find the most effective features for the proposed method is a subject for future investigations.

Numerous authors have applied clustering using multivariate Gaussian distributions for segmentation and classification of multispectral [52]–[55] and hyperspectral images [56], [57]. In particular, Acito *et al.* [57] segmented each of the first six PCA components of the 92-band MIVIS image using 1-D Gaussian mixture models and then fused partial segmentation results.

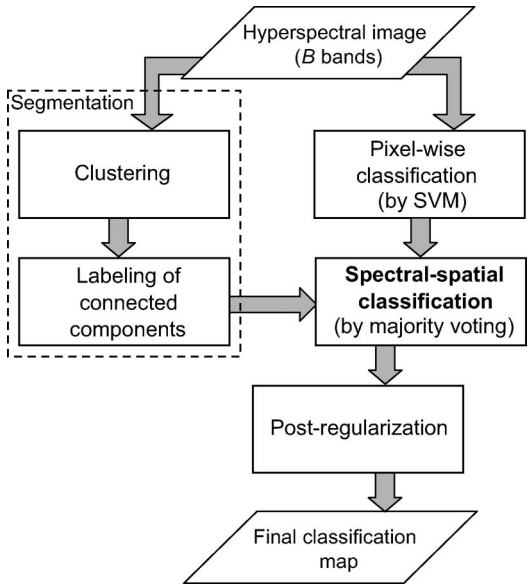

Fig. 1. Flowchart of the proposed spectral–spatial classification scheme.

Good segmentation results are reported in [57], although only visual results are presented, with no quantitative assessment. An oversegmentation effect was noted in these results, where different clusters corresponded to the same class in the ground scene.

B. Segmentation Using Clustering

The partitional clustering algorithm produces an exhaustive partitioning of the set of image pixels $\mathbf{X}$ into C clusters. Thus, each pixel has a numerical label of the cluster it belongs to. However, as no spatial information is used during the clustering procedure, pixels with the same cluster label can be connected in the image plane, thus forming a spatial region, or they can belong to disjoint regions within the spatial coordinates. Therefore, in order to obtain a segmentation map (where each connected spatial region has a unique label), a connected-component-labeling algorithm must be applied to the output image partitioning obtained by the clustering algorithm [26], [55]. This algorithm allocates different labels for disjoint regions in the image plane that were placed in the same cluster.

If the spatial dimensions of an image are not large, a classical connected-component algorithm using the union-find data structure can be used [58]. In the case of large-sized images, such algorithms as in [59] and [60] can be applied, as well as other sequential and parallel algorithms (references can be found for example in [60]). The *Segmentation* block in Fig. 1 thus consists of two stages: *Clustering* and *Labeling of connected components*.

The obtained segmentation map can be oversegmented, as reported, for example, in [57]. However, for the research presented in this paper, oversegmentation is not a crucial problem, since the final goal is not to obtain the segmentation result but to classify the image. Thus, we are searching for spatial regions of pixels that belong to the same physical object in order to incorporate this information into a spectral–spatial classifier. From this discussion, it is evident that undersegmentation is not desired. As oversegmentation is preferable to undersegmentation,

a four-neighborhood connectivity is preferable to use while performing the labeling of connected components.

III. Spectral–Spatial Classification Scheme

The flowchart of the proposed spectral–spatial classification scheme for hyperspectral data is shown in Fig. 1.

At the input, we have a B-band hyperspectral image $\mathbf{X} = \{\mathbf{x}_j \in \mathbf{R}^B, j = 1, 2, \ldots, n\}$ and a training set map.

The proposed spectral–spatial classifier is based on the *majority vote* rule. In previous studies, this approach was applied in a similar way in [61] for multispectral (four-band IKONOS) images and in [37] for hyperspectral data, giving a good performance. The approach is principally the combination of unsupervised segmentation and pixel wise classification results. The proposed method consists of the following steps (see Figs. 1 and 2).

1) *Segmentation:* A hyperspectral image is segmented into homogeneous regions using partitional clustering, as described in the previous section. The number of clusters ($C_{\min}/C_{\max}$ for the ISODATA and $C_{\max}$ for the EM) can be chosen based on the information about the considered image (i.e., how many groups of materials with similar spectra are present). $C_{\min}$ must be chosen not to be less than the number of classes. The upper bound of classes $C_{\max}$ can be chosen slightly superior to the number of classes. If less than $C_{\max}$ clusters are present in the image, both algorithms have the possibility to merge clusters.
2) *Pixel wise classification:* Independently of the segmentation procedure, a pixel wise classification of the image is performed. We propose to use an SVM classifier with the Gaussian radial basis function (RBF) kernel for this purpose, which has given good accuracies in classification of hyperspectral data [14], [15], [17]. Parameters of the classifier can be tuned by m-fold cross validation.
3) *Spectral–spatial classification:* Then, for every region in the segmentation map, all the pixels are assigned to the most frequent class within this region (we call this the *majority vote* rule).

   Please note that unlike in the fixed-window-based approach, the majority voting is not performed using a fixed neighborhood but using an adaptive neighborhood. For each pixel, the region it belongs to, as defined by the segmentation step, is used as its neighborhood for the majority voting on the spectral classification algorithm.
4) *PR:* Finally, spatial PR of the classification map is performed. The aim of this postprocessing step is to reduce the noise in the classification map after the majority vote procedure. For this purpose, the classification map is filtered, using the masks shown in Fig. 3 (that are 8- and 16-neighborhoods of a pixel, called Chamfer neighborhoods [62]). The PR is performed as follows.
   a) For every pixel in the classification map: If more than $T1$ neighbors in the eight-neighborhood [see Fig. 3(a)] have the class label L that is different from that of the considered pixel, assign this label L to the considered pixel. Perform this filtering until stability is reached (none of the pixels changes its label).

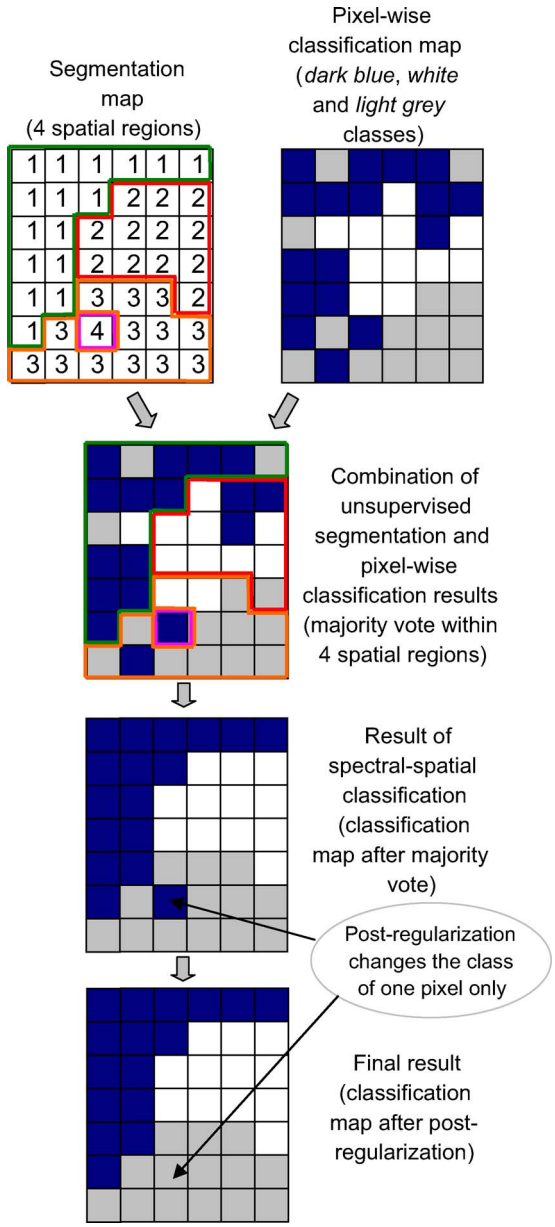

Fig. 2. Example of spectral–spatial classification.

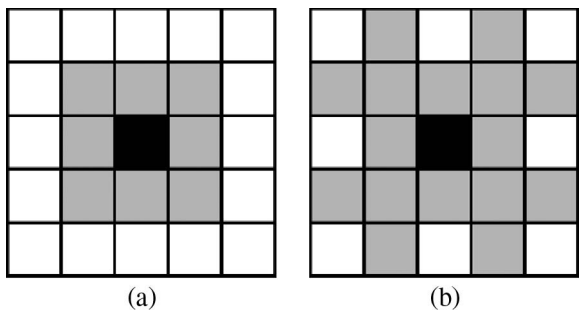

Fig. 3. Chamfer neighborhoods (in gray) for a black pixel: (a) 8 neighbors and (b) 16 neighbors.

   b) For every pixel: If more than $T2$ neighbors in the 16-neighborhood [see Fig. 3(b)] have the label L different from that of the considered pixel, assign the label L to the considered pixel. Perform this step until stability is reached.

c) Repeat regularization on the eight-neighborhood (with threshold $T3$).

The threshold values $T1-T3$ must be chosen to be equal or superior to a half of the number of pixels in the considered neighborhood in order to ensure the unique solution of the algorithm. The PR step results in more homogeneous regions in the classification map. However, the filtering of the classification map does not use any spectral pixel wise information. The effectiveness of this procedure depends on the sizes of the structures in the image. If the image resolution is not very high, the object in the image scene can be of the size of one or a few pixels. In this case, this object is in danger to be removed from the classification map by the PR. The filtering conditions can be restricted or relaxed by varying the threshold values $T1-T3$. If $Tj(j = 1, \ldots, 3)$ decreases, the regularization has a stronger effect. Hence, the results become more homogeneous. However, the risk to remove small but significant features increases.

Fig. 2 shows an example of the combination of spatial and spectral information using the proposed spectral–spatial classification method.

IV. Experimental Results and Discussion

A. Hyperspectral Image Data Set

Two different data sets were used for the experiments, with different contexts (one urban area and one agricultural area), different spatial resolutions (1.3 and 20 m per pixel, respectively), and different number of bands (103 and 220 bands, respectively). These two data sets and the corresponding results are presented in the next two sections.

B. Spectral–Spatial Classification of the University of Pavia Image

The *University of Pavia* image is of an urban area that was acquired by the ROSIS-03 optical sensor over the University of Pavia, Italy (provided by Deutsches Zentrum für Luft- und Raumfahrt). The image is 610 × 340 pixels, with a spatial resolution of 1.3 m per pixel. The number of data channels in the original recorded image is 115 (with a spectral range from 0.43 to 0.86 μm). The 12 most noisy channels have been removed, and the remaining 103 bands were used for the experiments. The reference data contain nine classes of interest. Table II details these classes, with the number of test and training samples for each class. Fig. 4(a) shows a three-band false color image. The reference data are shown in Fig. 4(b).

First, partitional clustering of the *University of Pavia* image was performed using the two techniques described in Section II.

For the ISODATA algorithm, considering that image pixels belong to one of the nine classes, we chose the number of clusters as $C_{\min} = 9$ and $C_{\max} = 10$. The algorithm resulted in splitting all the pixels into nine clusters. A higher upper bound of the number of clusters was also tested, but in that case, the algorithm merged clusters. Furthermore, the number of regions in the resulting segmentation map increased, and the segmentation results were not improved as compared to the original initialization.

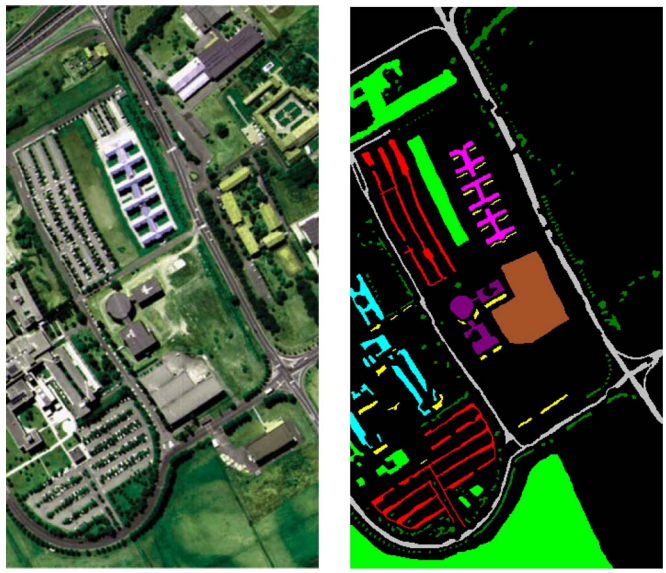

(a) (b)

Fig. 4. *University of Pavia* image. (a) Three-band color composite. (b) Reference data: Asphalt, meadows, gravel, trees, metal sheets, bare soil, bitumen, bricks, and shadow.

The EM clustering algorithm was performed with the *maximum* number of clusters $C_{\max} = 10$. As explained in Section II, the spectral dimension needs to be reduced before applying the EM algorithm. For feature reduction, a ten-band image was obtained by averaging over every ten neighboring bands.[1] At the output of the EM algorithm, the grouping of the image pixels into ten clusters was obtained. As for the ISODATA algorithm, the increase of the upper bound of the number of classes leads to the increase of the number of regions in the segmentation map, i.e., a more severe oversegmentation.

Fig. 5(a) and (b) shows the unsupervised classification maps obtained by the ISODATA and the EM algorithms, respectively. In each of these figures, different colors correspond to different clusters (which are not associated with any physical structures, as the maps are obtained by unsupervised techniques). As shown from the figures, the main spatial structures in the scene are well defined. Based on a visual inspection, the two obtained segmentation results are of comparable accuracies. The obtained unsupervised maps are clearly oversegmented, i.e., there are cases where the regions of pixels belonging to the same object were classified to different clusters (for instance, pixels from the region of *bare soil* in the center of the image were classified into several clusters).

The classical connected-component algorithm using the union-find data structure [58] was applied to these two unsupervised classification maps (using a four-neighborhood connectivity). The resulting segmentation maps contained 20 952 and 21 450 regions for the ISODATA and the EM techniques, respectively. In both cases, some regions contain a whole single physical object. For instance, a big structure belonging to the *metal sheets* class in the center of the image is mostly represented by one region. At the same time, a lot of small,

[1]The 103-band image was split into ten groups of ten bands; the three remaining bands were omitted.

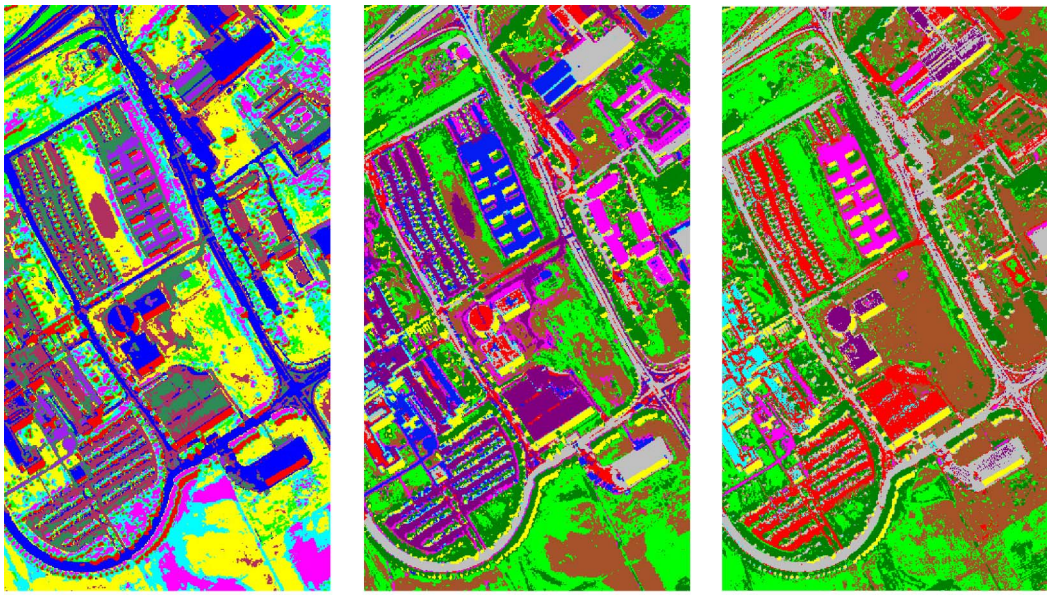

Fig. 5. Unsupervised classification maps for the *University of Pavia* image obtained by (a) ISODATA and (b) EM. (c) Supervised SVM classification map.

TABLE I
ASSESSMENT OF THE UNDERSEGMENTATION FOR THE *University of Pavia* IMAGE (FOR REGIONS CONTAINING PIXELS OF TWO DIFFERENT CLASSES; NUMBER OF PIXELS BELONGING TO EACH CLASS)

ISODATA		EM	
meadows	trees	meadows	trees
2	1	35	29
623	1	39	10
125	79	973	2
20	1	11	125
		1	90
asphalt	bricks		
1021	2		
trees	shadows		
1	57		

up to one pixel, regions are present, which explains the large number of regions in the obtained segmentation maps.

To assess quantitatively the accuracy of segmentation results, the analysis of undersegmentation/oversegmentation level was conducted. Two resulting segmentation maps and the image of the reference data [see Fig. 4(b)] were used for this purpose. In order to conclude if any undersegmentation is present in the considered segmentation results, images of a segmentation map and a reference data were superposed so that the reference data were partitioned into regions defined by the segmentation map. Then, the number of different classes within each region was computed. Nonlabeled pixels in the reference data were not taken into account (thus, if none of the pixels from a particular region was labeled, this region did not participate into the procedure of undersegmentation assessment).

For the undersegmentation assessment of the ISODATA segmentation map, 1560 regions were considered. Among them, 1554 regions only contained labeled pixels of the same class. Only six regions contained labeled pixels belonging to two different classes. For the EM segmentation map, among the 2029 considered regions, only 5 regions contained pixels from 2 different classes; other regions were not undersegmented. Table I gives the detailed information about undersegmented regions. As shown from the table, the undersegmentation occurs mostly between classes *meadows* and *trees*. From this analysis, it can be concluded that the undersegmentation is almost not present in the obtained results. Therefore, the segmentation maps can, as a matter of fact, be used in the proposed spectral–spatial classification scheme.

Furthermore, in order to investigate the level of oversegmentation, we computed how many regions from the segmentation map each connected component in the reference data contained (if only a part of the region is present within the considered connected component, it was also counted as one region with this component). The reference data contained 265 connected components. Fig. 6 shows results for both ISODATA and EM segmentation maps (in a logarithmic scale). For the ISODATA (EM) segmentation results, 120 (163), 70 (56), and 25 (12) connected components from the reference data contained 1, 2, and 3 regions from the segmentation map, respectively. Thus, for both segmentation results, more that 81% of the connected components contained no more than 3 regions from the segmentation map. For several connected components, the number of regions that they contain is somewhat larger. In most cases, these components contain a large number of pixels (in Fig. 6, the total number of pixels for each connected component in reference data is also visualized). The average ratio of the number of pixels in the connected component and the number of regions within the component is equal to 16.78 and 21.46 for the ISODATA and the EM segmentation results, respectively. Based on this, it can be concluded that the oversegmentation is present in the obtained segmentation results. However, as explained in Section II, oversegmented maps of spatial regions can be used in the proposed spectral–spatial classification scheme without the risk to worsen classification accuracies obtained by the pixel wise classification.

After the initial segmentation step, the pixel wise classification step was performed using the multiclass pairwise (one versus one) SVM classifier, with the Gaussian RBF kernel

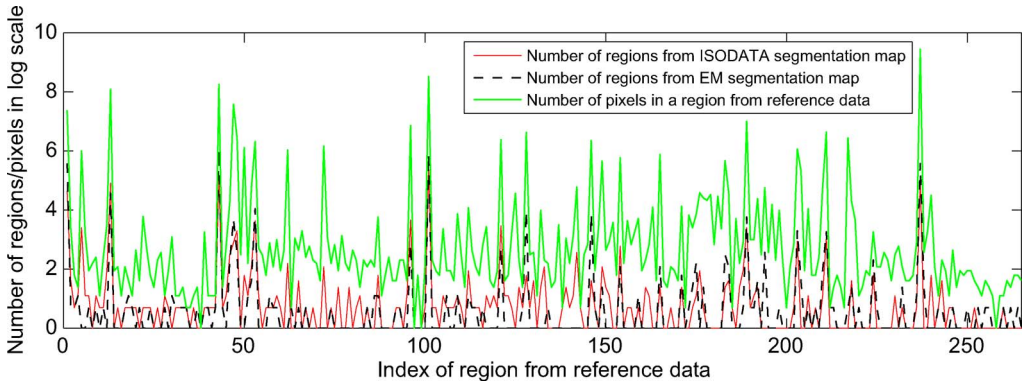

Fig. 6. Assessment of oversegmentation: Number of regions from the segmentation map contained in the connected components from the reference data and total number of pixels in each connected component from the reference data. Results are shown in a logarithmic scale.

TABLE II
INFORMATION CLASSES, TRAINING-TEST SAMPLES, AND CLASS-SPECIFIC ACCURACIES IN PERCENTAGE FOR THE *University of Pavia* IMAGE ("*PR*" MEANS THE INCLUSION OF A PR STEP)

Class		Samples		SVM		SVM+ISODATA		SVM+EM		EMP
No	Name	Train	Test		*PR*		*PR*		*PR*	
1	asphalt	548	6304	84.93	90.13	92.16	94.40	90.72	93.45	**95.36**
2	meadows	540	18146	70.79	73.73	87.07	87.45	92.73	**93.78**	80.33
3	gravel	392	1815	67.16	68.93	61.43	61.32	82.09	82.53	**87.61**
4	trees	524	2912	97.77	98.76	98.59	98.63	99.21	**99.38**	98.37
5	metal sheets	265	1113	99.46	99.91	99.46	99.91	**100**	**100**	99.48
6	bare soil	532	4572	92.83	96.87	97.38	**97.88**	96.78	97.38	63.72
7	bitumen	375	981	90.42	93.68	99.69	**100**	92.46	94.19	98.87
8	bricks	514	3364	92.78	97.41	98.69	**99.02**	97.80	98.31	95.41
9	shadows	231	795	98.11	**98.62**	97.86	97.86	97.74	97.86	97.68

(by means of the LIBSVM library [63]). The optimal parameters C and γ were chosen by fivefold cross validation: $C = 128$ and $\gamma = 0.125$. The resulting classification map is shown in Fig. 5(c). The results of pixel wise classification were combined with the segmentation results using a *majority vote* approach (as explained in Section III).

The concluding PR step was performed on the pixel wise classification map and on two maps obtained by the spectral–spatial classification. Based on experimental results, we have chosen the threshold values $T1 = T3 = 5$ and $T2 = 12$. These values are considered as being a good tradeoff for filtering the noise while minimizing the risk of losing small but significant objects in the classification map.

Table III gives the global classification accuracies for the pixel wise SVM and the combined spectral–spatial classification before and after PR. The following measures of accuracy were used: overall accuracy (OA is the percentage of correctly classified pixels), average accuracy (AA is the mean of class-specific accuracies, i.e., the percentage of correctly classified pixels for each class), and kappa coefficient (κ, formula can be found in [39]). The class-specific accuracies are presented in Table II. Fig. 7 shows the classification maps for the pixel wise SVM and the spectral–spatial classification after the PR step. In order to compare the obtained results with previous works that used an SVM and spatial information for hyperspectral image classification, we have included in Tables II and III accuracies of mathematical morphology-based classification of the *University of Pavia* image using SVM, principal components, and extended morphological profiles (EMPs); results are taken from the work of Plaza *et al.* [64], where the same training and testing samples were used for classification. This method was recently proposed by Benediktsson *et al.* [65] and has given good classification accuracies. Other results of spectral–spatial classification of the considered image can be found in [15], [19], and [66].

As can be seen from Table III, the SVM classifier gives high classification accuracies. The incorporation of the segmentation map obtained by clustering techniques into spectral–spatial classifier significantly improves the classification accuracies. The best global accuracies are achieved when using the spectral–spatial classifier based on the clustering by the EM algorithm with the PR step. In this case, the OA is improved by 13.7% and the AA improved by 7.0% compared to the pixel-wise SVM classification. The accuracies were substantially improved after spatial PR, with the improvement being more significant when this step is performed after a pixel wise SVM classification. This result meets expectations as the spectral–spatial classification already removes noise in the classification map, leading to more homogeneous regions. Therefore, less noise is left to be removed by means of the PR step.

The spectral–spatial classification improves the classification accuracies for almost all the classes (see Table II), except for the class *shadows*. For this class, the PR of the pixel wise SVM classification map improves the classification accuracy slightly. However, when performing the spectral–spatial classification, the classification accuracy is nonsignificantly reduced (two more pixels are misclassified compared to the results of the pixel wise classification). For the other classes, classification accuracies are improved in a range of 0.5%–23.0%. The spectral–spatial classification based on the ISODATA clustering gives the best classification accuracies for the classes *bare soil*, *bitumen*, and *bricks*, while for the classes *meadows*, *trees*, and

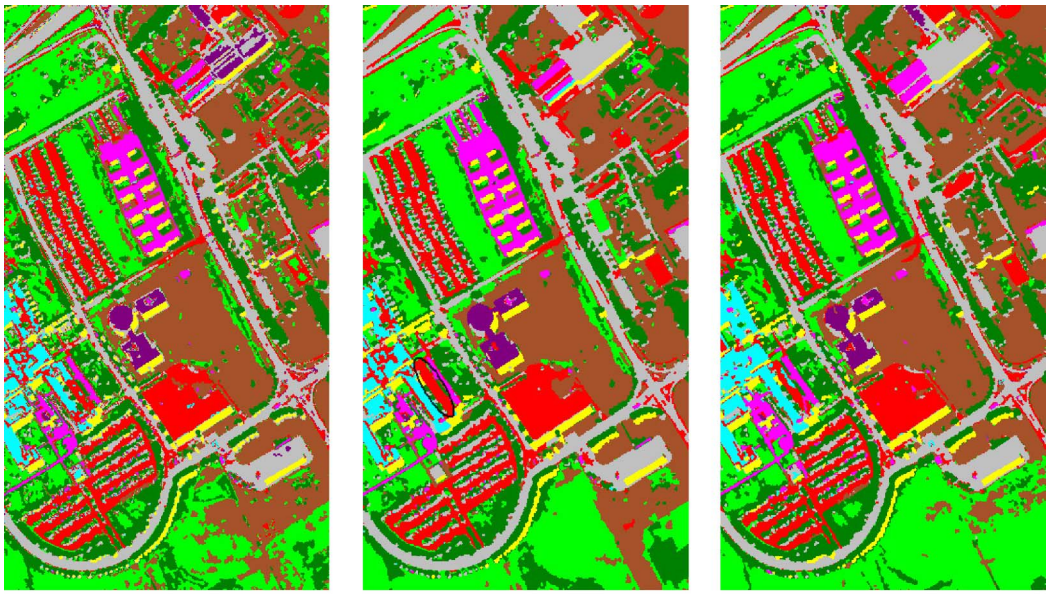

Fig. 7. Classification maps for the *University of Pavia* image after PR: (a) Pixel wise SVM classification, (b) SVM + ISODATA, and (c) SVM + EM.

TABLE III
GLOBAL CLASSIFICATION ACCURACIES IN PERCENTAGE FOR THE *University of Pavia* IMAGE ("*after PR*" MEANS THE INCLUSION OF A PR STEP)

Method		OA	AA	κ
Pixel-wise SVM		81.01	88.25	75.86
	after PR	84.27	90.89	79.90
SVM+ISODATA		90.57	92.48	87.62
	after PR	91.20	92.94	88.43
SVM+EM		93.59	94.39	91.48
	after PR	**94.68**	**95.21**	**92.92**
EMP		85.22	90.76	80.86

metal sheets, the EM clustering algorithms led to the best results. In particular, the class *meadows* is much more accurately classified when the spatial information is used (improvement of the classification accuracy by 23.0% when using the EM clustering). This class describes mostly large regions in the image. Furthermore, the incorporation of the information from the segmentation map results in much more homogeneous regions. The classes *bitumen* and *metal sheets* were identified with a 100% accuracy by the spectral–spatial classification using the ISODATA and the EM, respectively.

The use of spatial information in a classifier, by incorporating a segmentation map and performing PR, significantly reduces noise in the classification map (see Figs. 5(c) and 7). The classification maps obtained by the spectral–spatial classification before the PR are not shown as these maps are very similar to those after the PR. That is explained by the fact that majority voting within regions of the segmentation map has already removed most of the noise in the classification map, as previously mentioned. In Fig. 7(b), it can be noted that one object belonging to the class *gravel* (marked by the black ellipse in the figure) was wrongly assigned to the class *bricks*. In that case, the segmentation by ISODATA helped in identifying this object as one homogeneous object (the ISODATA identified two big regions within this object). However, as the pixel wise SVM classifier has assigned most of the pixels to the class *bricks*, the whole object was assigned to this class by the *majority vote* rule. Another approach for combination of spatial and spectral information in classification could be more suitable in this case.

These results have shown that the proposed spectral–spatial classification scheme, using majority voting within the regions in the segmentation map obtained by partitional clustering techniques, leads to improved classification accuracies and more homogeneous objects in the resulting classification maps when compared to the pixel wise classification. The approach is particularly suitable for classification of large spatial structures in the image. However, when including the spatial information from the segmentation map or from the closest neighborhoods, we risk to assimilate small structures in the image with the larger structures in their neighborhood (particularly if their spectral responses are not very different). Therefore, small structures are in danger of disappearing in the final classification map when performing the spectral–spatial classification. Accurate segmentation results help to overcome this problem.

The classification accuracies shown in this paper are higher than all previous results that we have found in the literature for this particular data set [15], [19], [64], [66]. In particular, when we compare the obtained results with the recent results of spectral–spatial classification using the SVM and EMPs (see Tables II and III), the proposed approach leads to significantly higher global accuracies and to higher class-specific accuracies for most of the classes. Thus, the segmentation using clustering, enabling the inclusion of the spatial information in a classifier, appears to be an appropriate technique for finding homogeneous objects in a hyperspectral image of an urban area.

C. Spectral–Spatial Classification of the Indiana Image

The proposed spectral–spatial classification scheme was tested on the *Indiana* image of an agricultural area, with more bands (number of bands $B = 220$) and a lower spatial resolution, as compared to the *University of Pavia* image.

TABLE IV
INFORMATION CLASSES, NUMBER OF LABELED SAMPLES, AND CLASS-SPECIFIC ACCURACIES IN PERCENTAGE FOR THE *Indiana* IMAGE ("*PR*" MEANS THE INCLUSION OF A PR STEP)

Class		No. of samples in reference data	SVM		SVM+ISODATA		SVM+EM	
No	Name			*PR*		*PR*		*PR*
1	Corn-no till	1434	74.59	**83.27**	79.32	80.48	71.65	71.42
2	Corn-min till	834	64.58	78.30	84.95	**88.02**	84.15	86.68
3	Corn	234	58.77	81.99	75.83	**85.31**	60.66	65.40
4	Soybeans-no till	968	69.76	78.81	83.85	**84.19**	82.02	82.47
5	Soybeans-min till	2468	79.21	93.88	93.16	95.77	95.05	**97.12**
6	Soybeans-clean till	614	75.41	89.69	85.17	89.87	90.05	**92.59**
7	Alfalfa	54	32.65	**36.73**	12.24	6.12	0	0
8	Grass/pasture	497	87.05	90.18	93.08	93.75	93.97	**95.31**
9	Grass/trees	747	92.72	97.62	94.80	96.88	99.11	**99.26**
10	Grass/pasture-mowed	26	29.17	29.17	**91.67**	**91.67**	0	0
11	Hay-windrowed	489	96.37	97.96	97.51	97.51	**99.09**	**99.09**
12	Oats	20	**22.22**	**22.22**	16.67	11.11	0	0
13	Wheat	212	90.58	97.38	93.19	98.43	**98.95**	**98.95**
14	Woods	1294	91.07	95.88	97.17	**97.85**	95.36	96.82
15	Bldg-Grass-Tree-Drives	380	65.50	78.36	79.53	**85.38**	69.30	79.24
16	Stone-steel towers	95	84.88	84.88	86.05	**87.21**	86.05	86.05

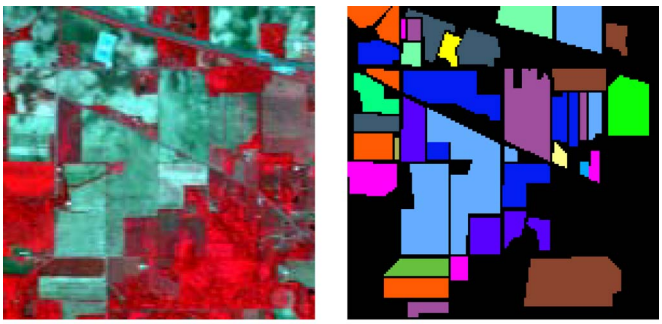

(a) (b)

Fig. 8. *Indiana* image. (a) Three-band color composite (bands 50, 27, and 17). (b) Reference data: Corn-no till, corn-min till, corn, soybeans-no till, soybeans-min till, soybeans-clean till, alfalfa, grass/pasture, grass/trees, grass/pasture-mowed, hay-windrowed, oats, wheat, woods, bldg-grass-tree-drives, and stone-steel towers.

The *Indiana* image was recorded by the AVIRIS sensor over the Indian Pines test site in Northwestern Indiana [38]. The image has a spatial dimension of 145 × 145 pixels, and the spatial resolution is 20 m per pixel. The full spectral range of 220 channels was used for the experiments. Sixteen classes of interest are considered, which represent mostly different types of crops and are detailed in Table IV, with a number of samples for each class in the reference data. A three-band false color image and the reference data are shown in Fig. 8. We have chosen randomly 10% of the samples for each class from the reference data as training samples, and the remaining samples composed the test set.

Both the ISODATA and the EM algorithm were applied to perform a partitional clustering of the image. The ISODATA was performed with $C_{\min} = 16$ and $C_{\max} = 19$. The EM clustering was applied to the 22-band image (obtained by averaging over every 10 neighboring bands of the original data) with $C_{\max} = 17$. Both algorithms grouped the image pixels into 17 clusters.

The unsupervised classification maps obtained by the ISODATA and the EM algorithm are shown in Fig. 9(a) and (b), respectively (different colors correspond to different clusters). As in the previous experiment, the images are oversegmented, but here, the spatial structures, corresponding to the crop fields, can be recognized. We can also see [when comparing these classification maps with the reference data in Fig. 8(b)] that some pixels belonging to different classes are classified by the clustering techniques to the same cluster. For instance, in Fig. 9(a), at the center of the image, there are two large light-green regions of pixels that belong to the same cluster. These regions represent different crop fields: *soybeans-no till* (class 4, violet color in the reference data) and *soybeans-min till* (class 5, light-blue color in the reference data). The spectral responses of the pixels from these two classes are similar, and the clustering algorithms group them to the same cluster. However, as we are interested in obtaining a segmentation map, where the image is partitioned into regions, without any additional information about the region, it is important that these two regions of pixels belonging to the same cluster are disconnected in space.

To obtain segmentation maps, connected-component labeling of the unsupervised classification maps was performed using the same algorithm as for the previous data set and four-neighborhood connectivity. The resulting segmentation maps for the ISODATA and the EM techniques contained 3977 and 3728 regions, respectively. As explained for the *University of Pavia* image, the segmentation using clustering produces a map with comparatively large regions along with a lot of very small and one-pixel regions.

Multiclass, one versus one, SVM classification was performed on the original image using the Gaussian RBF kernel. The parameters C and γ were determined by fivefold cross validation, which gave $C = 1024$ and $\gamma = 2^{-7}$. Fig. 9(c) shows the obtained classification map. After the pixel wise SVM classification, majority voting within the regions from each of the segmentation maps was performed. Then, PR was applied to the two classification maps obtained by the spectral–spatial classification and to the pixel wise classification map (with $T1 = T3 = 5$ and $T2 = 12$).

Tables IV and V give the class-specific and the global classification accuracies, respectively, for the pixel wise and the spectral–spatial classification, without and with the PR step. The classification maps for the pixel wise and the spectral–spatial classification after the PR are shown in Fig. 10.

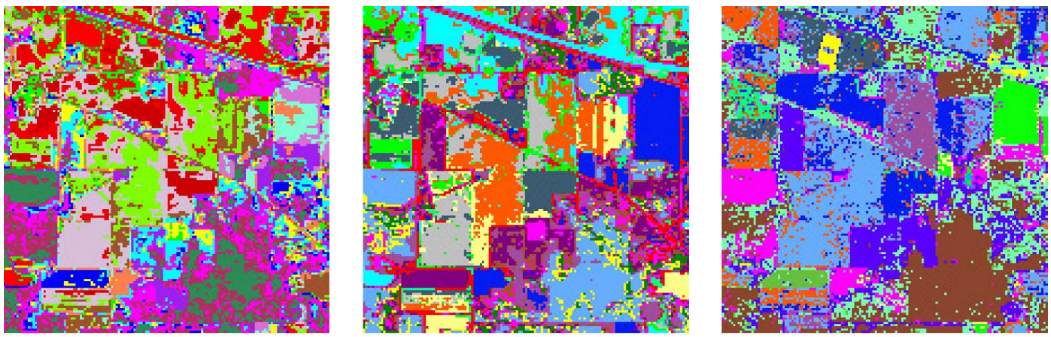

Fig. 9. Unsupervised classification maps for the *Indiana* image obtained by (a) ISODATA and (b) EM. (c) Supervised SVM classification map.

TABLE V
GLOBAL CLASSIFICATION ACCURACIES IN PERCENTAGE FOR THE *Indiana* IMAGE ("*after PR*" MEANS THE INCLUSION OF A PR STEP)

Method		OA	AA	κ
Pixel-wise SVM		78.76	69.66	75.73
	after PR	88.58	77.27	86.93
SVM+ISODATA		88.53	79.01	86.90
	after PR	**90.64**	**80.60**	**89.31**
SVM+EM		87.25	70.34	85.43
	after PR	88.83	71.90	87.24

Here, it is worth mentioning that the low spatial resolution of the *Indiana* image leads to the presence of highly mixed pixels. This makes the tasks of the unsupervised segmentation by clustering and the supervised SVM classification more complicated. We previously discussed an example where pixels belonging to different classes were grouped to the same cluster. One of the reasons of this inaccuracy in the unsupervised classification could be the presence of spectrally mixed pixels in the image.

Another complication of the segmentation and classification tasks is caused by a significant difference in the number of pixels in the image and in the reference data for different classes, which varies in the reference data from 20 to 2468 pixels per class. Some classes represent big crop fields, while others represent very small fields.

The 10% of samples for each class were chosen randomly from the reference data as a training set for the SVM classifier. Therefore, some classes were represented by a few samples in the training set (two samples only for the class *oats*), which probably do not provide a fair-enough representation of the class.

Despite these complications, the SVM classifier correctly classified 78.76% of pixels from the test set. The classification accuracies for the classes *alfalfa*, *grass/pasture-mowed,* and *oats*, which were represented by only a few samples in the training set (further called as *small classes*), are low (less than 33%). Consequently, the average classification accuracy is only 69.66%.

As can be seen from Tables IV and V, the simple filtering (PR) improves the classification accuracies significantly. The OA and AA are improved by 9.8% and 7.6%, respectively, after the PR step of the pixel wise SVM classification. Accuracies of almost all classes are significantly improved, except for some *small classes* (for them, the accuracies are not changed, but for the class *alfalfa*, the accuracy is improved). This is explained by the fact that most of the classes in the image represent large crop fields, and the simple filtering makes these regions of fields homogeneous, thereby improving the classification accuracies.

The best global accuracies are obtained when performing the spectral–spatial classification using ISODATA clustering and the PR. In that case, the OA and AA are improved by 11.9% and 10.9%, respectively, compared to the pixel wise SVM classification. Almost all the class-specific accuracies are improved. When looking at the results for the *small classes*, the classification accuracy was significantly improved for the class *grass/pasture-mowed* (from 29.17% to 91.67%), while for the classes *alfalfa* and *oats*, accuracies are reduced (the problem of the spectral–spatial classification for the *small classes* will be discussed hereinafter).

The OA for the spectral–spatial classification using the EM clustering is slightly lower than that when using the ISODATA clustering technique. The EM clustering approach led to the best classification results for some classes (six classes, as can be seen from Table IV). However, for the *small classes* (*alfalfa*, *grass/pasture-mowed*, and *oats*), none of the pixels from the test set was identified correctly by this classifier, and that reduced the average classification accuracy. The potential misclassification of *small classes* is actually caused by the low spatial resolution of image, the presence of classes with similar spectral responses, and the small number of samples per class in the image/training set. The two main reasons for the problem of the classification of these classes can be defined.

1) Very small crop fields of *grass/pasture-mowed* and *oats* were assimilated with their neighboring regions (which represented the big fields of *grass/pasture* and *grass/trees*, respectively) when performing the segmentation and the majority voting.
2) For the class *alfalfa*, the EM clustering grouped the pixels from the *alfalfa* and the *hay-windrowed* (a big light-green field in the right part of the image) fields into the same cluster. And the pixel wise SVM classifier assigned the majority of the *alfalfa* pixels from the test set to the class *hay-windrowed*, as the spectral responses of these two classes were similar [see Figs. 9(b) and (c) and 10(c)]. The segmentation map contains a separate region that corresponds to the *alfalfa* field, but according to the *majority vote* rule, all the pixels were assigned to *hay-windrowed*, which is an incorrect class.

As mentioned before, one of the problems with the partitional clustering techniques concerns the dependence of the results on

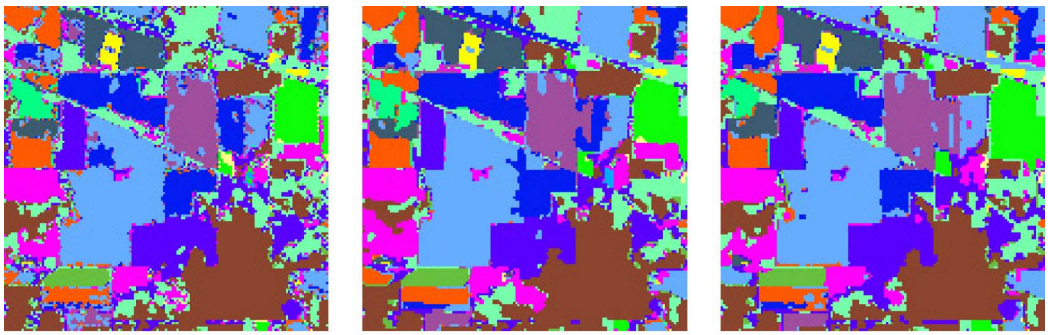

Fig. 10. Classification maps for the *Indiana* image after PR. (a) Pixel wise SVM classification, (b) SVM + ISODATA, and (c) SVM + EM.

TABLE VI
PROCESSING TIME IN SECONDS FOR CLUSTERING ALGORITHMS AND SVM CLASSIFICATION FOR THE *University of Pavia* IMAGE (B—DIMENSIONALITY OF PATTERNS; I—NUMBER OF ITERATIONS)

Algorithm	B	I	time
ISODATA	103	8	185
EM	10	3	3
SVM (training+classification)	103	-	3339

the initialization. For the two considered algorithms, C cluster centers are initially chosen randomly from a set of pixels, and the remaining pixels are assigned to the cluster with the closest center. If one class contains very few pixels compared to the other classes, the probability is low that one of its pixels will be chosen at the start as a cluster center. Then, when centers are recomputed and pixels are reassigned, pixels from this *small class* can compose a separate class only if their spectral response is very different from that of the other classes. However, otherwise, if there is a class with a large number of pixels that have a similar spectral response, pixels from the *small class* will probably be grouped to the same cluster with the *large class*. Furthermore, the considered clustering algorithms have mechanisms to delete clusters, based on the number of pixels in the cluster. For instance, the EM algorithm eliminates a cluster if the number of pixels in this cluster is less than the dimensionality of the pixels (as the covariance matrix of every cluster must be computed at every iteration). It can also be an obstacle to identify the pixels from a *small class* to a separate cluster (if this cluster is very small, it can be eliminated). All these reasons led to either 0% or low classification accuracies for the *small classes* when classifying the *Indiana* image.

The experimental results on the *Indiana* image (see Figs. 9(c) and 10) have confirmed that the proposed spectral–spatial classification method based on the partitional clustering results in a classification map with more homogeneous regions when compared to pixel wise classification. The proposed scheme is particularly suitable for classification of images with large spatial structures. Furthermore, it is also suitable if different classes have dissimilar spectral responses and a comparable number of pixels (of the same order).

More classification results for the *Indiana* image can be found in [64] and [67] for comparison. The accuracies in the referenced works are not directly compared with those given in this paper because different training–testing sets are used. However, it can be concluded that our approach performs well compared to other previously proposed classification approaches.

D. Consideration of Computational Complexity for the Spectral–Spatial Classification Method

When comparing the results of two classifiers, an important issue is the computational complexity and the processing time of each classifier. Although the pixel wise SVM classifier gives good classification accuracies, it is a computationally demanding algorithm for high-dimensional data and/or when the number of training samples is large [19], [68]. The training part of the SVM classification is the most time-consuming, in particular the tuning of parameters by cross validation. We conducted experiences on an Intel Core 2 Duo 2.40-GHz processor with 3.5-GB RAM. The processing times for the training and classification parts of the *University of Pavia* image by means of the LIBSVM library were 3240 and 99 s, respectively. However, in recent works, methods and parallel implementations to speed up the SVM training and classification have been proposed [64], [69], [70], [71].

When we perform a segmentation of an image by clustering and combine spatial information with the results of pixel wise classification, the processing time obviously increases, when compared to pixel wise classification only. However, the partitional clustering algorithms are much less time-consuming than the SVM classification algorithm. The computational complexity of both the ISODATA and EM clustering algorithms is $O(nCB^2I)$, where I is the number of iterations (until the convergence of algorithm). Therefore, we can say that the processing time depends mainly on the dimensions of the image. Table VI summarizes the processing time for clustering algorithms versus SVM classification for the *University of Pavia* image as a function of dimensionality of patterns and number of iterations. These results are not directly comparable, as different software packages were used (ENVI software to apply ISODATA and the C++ implementation for the EM algorithm). However, it can be seen that the EM algorithm ran much faster than the ISODATA algorithm mainly because of a lower spectral dimensionality. Furthermore, the processing time for the used clustering techniques is significantly smaller than the time for the SVM classification (although, in general, this ratio depends on the number of training samples and the clustering algorithm). In addition, as was mentioned before, efficient implementations of the clustering algorithms are possible.

In addition, it must be mentioned that the segmentation and pixel wise classification of an image can be executed at the same time on different processing units (since none of these tasks depends on the results of another task). In that case, after the pixel wise classification is completed, majority voting and PR are applied, which are both very fast algorithms. Furthermore, as shown earlier, the incorporation of spatial information significantly improves accuracies. When the spatial information is incorporated, the classification in the pixel wise classification step can be speeded up by sacrificing some percentage of the classification accuracy. That can be achieved either by decreasing the number of pixels in the training set or by using another less time-consuming classifier than the SVM for pixel wise classification.

V. Conclusion

A new spectral–spatial classification scheme for hyperspectral images was presented. The proposed method combines the results of a pixel wise SVM classification and a segmentation map obtained by partitional clustering. This is achieved by performing a majority voting on the pixel wise spectral classification using adaptive neighborhoods defined by the segmentation map. The use of both the ISODATA and the Gaussian mixture resolving techniques for hyperspectral image segmentation was investigated. The incorporation of spatial information from the segmentation in the classifier produces a classification map with more homogeneous regions, as compared to only pixel wise classification of hyperspectral data. Here, the remaining noise in the classification map was further reduced by a fixed-window-based postfiltering.

Experimental results have shown that the proposed method improves the classification accuracies and provides classification maps with more homogeneous regions when compared to pixel wise classification.

The developed scheme is particularly suitable for classification of images with large spatial structures, when spectral responses of the different classes are dissimilar and the classes contain a comparable number of pixels. The drawback of the proposed method is that when including spatial information from the segmentation map or from the closest neighborhoods in a classifier, small spatial structures face a risk of being assimilated with larger neighboring structures if the spectral responses are not significantly different.

In the future, we will investigate the use of feature extraction to find the most effective features to be used in the clustering. In particular, applying feature reduction transformations enables the reduction of the spectral dimension while the most important information for classification is preserved. That may lead to a better distinction between classes and thus to better segmentation results.

Acknowledgment

The authors would like to thank the anonymous reviewers for their constructive comments that helped improve this paper significantly. The authors would also like to thank Deutsches Zentrum für Luft- und Raumfahrt, P. Gamba from the University of Pavia, Italy, and D. Landgrebe from Purdue University, USA, for providing the hyperspectral data. The authors would also like to thank I. Kåsen, T. V. Haavardsholm, and T. Skauli from FFI, Norway, for a fruitful discussion about the EM algorithm.

References

[1] R. O. Green, M. L. Eastwood, C. M. Sarture, T. G. Chrien, M. Aronsson, B. J. Chippendale, J. A. Faust, B. E. Pavri, C. J. Chovit, M. S. Solis, M. R. Olah, and O. Williams, "Imaging spectroscopy and the Airborne Visible/Infrared Imaging Spectrometer (AVIRIS)," *Remote Sens. Environ.*, vol. 65, no. 3, pp. 227–248, Sep. 1998.

[2] L. Rickard, W. Basedow, E. Zalewski, P. Silverglate, and M. Landers, "HYDICE: An airborne system for hyperspectral imaging," in *Proc. SPIE Imaging Spectrometry Terrestrial Environ.*, 1993, vol. 1937, pp. 173–179.

[3] B. Stevenson, R. O'Connor, W. Kendall, A. Stocker, W. Schaff, R. Holasek, D. Even, D. Alexa, J. Salvador, M. Eismann, R. Mack, P. Kee, S. Harris, B. Karch, and J. Kershenstein, "The civil air patrol ARCHER hyperspectral sensor system," in *Proc. SPIE Airborne ISR Syst. Appl. II*, 2005, vol. 5787, pp. 17–28.

[4] T. Cocks, R. Jenssen, A. Stewart, I. Wilson, and T. Shields, "The HyMap airborne hyperspectral sensor: The system, calibration and performance," in *Proc. 1st EARSEL Workshop Imaging Spectroscopy*, Oct. 1998, pp. 37–43.

[5] J. Pearlman, C. Segal, L. Liao, S. Carman, M. Folkman, B. Browne, L. Ong, and S. Ungar, "Development and operations of the EO-1 Hyperion imaging spectrometer," in *Proc. SPIE Earth Observing Syst. V*, 2000, vol. 4135, pp. 243–253.

[6] C.-I. Chang, *Hyperspectral Imaging: Techniques for Spectral Detection and Classification*. Dordrecht, The Netherlands: Kluwer, 2003.

[7] D. A. Landgrebe, *Signal Theory Methods in Multispectral Remote Sensing*. New York: Wiley, 2003.

[8] P. K. Goel, S. O. Prasher, R. M. Patel, J. A. Landry, R. B. Bonnell, and A. A. Viau, "Classification of hyperspectral data by decision trees and artificial neural networks to identify weed stress and nitrogen status of corn," *Comput. Electron. Agric.*, vol. 39, no. 2, pp. 67–93, 2003.

[9] H. Zhou, Z. Mao, and D. Wang, "Classification of coastal areas by airborne hyperspectral image," in *Proc. SPIE Opt. Technol. Atmos., Ocean, Environ. Stud.*, May 2005, vol. 5832, pp. 471–476.

[10] S. Subramanian, N. Gat, M. Sheffield, J. Barhen, and N. Toomarian, "Methodology for hyperspectral image classification using novel neural network," in *Proc. SPIE Algorithms Multispectral Hyperspectral Imagery III*, A. E. Iverson, S. S. Shen, Eds., Aug. 1997, vol. 3071, pp. 128–137.

[11] H. Yang, F. V. D. Meer, W. Bakker, and Z. J. Tan, "A back-propagation neural network for mineralogical mapping from AVIRIS data," *Int. J. Remote Sens.*, vol. 20, no. 1, pp. 97–110, 1999.

[12] C. Hernández-Espinosa, M. Fernández-Redondo, and J. Torres-Sospedra, "Some experiments with ensembles of neural networks for classification of hyperspectral images," in *Proc. ISNN*, vol. 1, 2004, pp. 912–917.

[13] C. Vaiphasa, "Innovative genetic algorithm for hyperspectral image classification," in *Proc. Int. Conf. Map Asia*, 2003, p. 20.

[14] G. Camps-Valls and L. Bruzzone, "Kernel-based methods for hyperspectral image classification," *IEEE Trans. Geosci. Remote Sens.*, vol. 43, no. 6, pp. 1351–1362, Jun. 2005.

[15] M. Fauvel, "Spectral and spatial methods for the classification of urban remote sensing data," Ph.D. dissertation, Grenoble Inst. Technol., Grenoble, France, 2007.

[16] J. A. Gualtieri and R. F. Cromp, "Support vector machines for hyperspectral remote sensing classification," *Proc. SPIE*, vol. 3584, pp. 221–232, Jan. 1998.

[17] M. Fauvel, J. Chanussot, and J. A. Benediktsson, "Evaluation of kernels for multiclass classification of hyperspectral remote sensing data," in *Proc. ICASSP*, May 2006, pp. II-813–II-816.

[18] M. Pesaresi and J. A. Benediktsson, "A new approach for the morphological segmentation of high-resolution satellite imagery," *IEEE Trans. Geosci. Remote Sens.*, vol. 39, no. 2, pp. 309–320, Feb. 2001.

[19] M. Fauvel, J. Chanussot, J. A. Benediktsson, and J. R. Sveinsson, "Spectral and spatial classification of hyperspectral data using SVMs and morphological profiles," *IEEE Trans. Geosci. Remote Sens.*, vol. 46, no. 10, pp. 3804–3814, Oct. 2008.

[20] A. Farag, R. Mohamed, and A. El-Baz, "A unified framework for map estimation in remote sensing image segmentation," *IEEE Trans. Geosci. Remote Sens.*, vol. 43, no. 7, pp. 1617–1634, Jul. 2005.

[21] R. Jain, R. Kasturi, and B. G. Schunck, *Machine Vision*, ser. McGraw-Hill Series in Computer Science. New York: McGraw-Hill, 1995.

[22] K. Fu and J. Mui, "A survey on image segmentation," *Pattern Recognit.*, vol. 13, no. 1, pp. 3–16, 1981.

[23] P. Lambert and L. Macaire, "Filtering and segmentation: The specifity of color images," in *Proc. Int. Conf. Color Graph. Image Process.*, 2000, vol. 1, pp. 57–64.

[24] R. Haralick and L. Shapiro, "Survey: Image segmentation techniques," *Comput. Vis. Graph. Image Process.*, vol. 29, no. 1, pp. 100–132, 1985.

[25] P. Paclík, R. Duin, G. V. Kempen, and R. Kohlus, "Segmentation of multi-spectral images using the combined classifier approach," *Image Vis. Comput.*, vol. 21, no. 6, pp. 473–482, Jun. 2003.

[26] A. K. Jain, M. N. Murty, and P. J. Flynn, "Data clustering: A review," *ACM Comput. Surv.*, vol. 31, no. 3, pp. 264–323, Sep. 1999.

[27] S. Lee and M. Crawford, "Unsupervised multistage image classification using hierarchical clustering with a Bayesian similarity measure," *IEEE Trans. Image Process.*, vol. 14, no. 3, pp. 312–320, Mar. 2005.

[28] G. Ball and D. Hall, "ISODATA, a novel method of data analysis and classification," Stanford Univ., Stanford, CA, Tech. Rep. AD-699616, 1965.

[29] A. P. Dempster, N. M. Laird, and D. B. Rubin, "Maximum likelihood from incomplete data via the EM algorithm," *J. R. Stat. Soc. B*, vol. 39, no. 1, pp. 1–38, 1977.

[30] N. B. Venkateswarlu and P. S. V. S. K. Raju, "Fast ISODATA clustering algorithms," *Pattern Recognit.*, vol. 25, no. 3, pp. 335–342, Mar. 1992.

[31] Y. Tarabalka, T. V. Haavardsholm, I. Kåsen, and T. Skauli, "Real-time anomaly detection in hyperspectral images using multivariate normal mixture models and GPU processing," *J. Real-Time Image Process.*, pp. 1–14, 2008. DOI:10.1007/s11554-008-0105-x.

[32] F. Lafarge, X. Descombes, and J. Zerubia, "Textural kernel for SVM classification in remote sensing: Application to forest fire detection and urban area extraction," in *Proc. ICIP*, Sep. 2005, vol. 3, pp. III-1096–III-1099.

[33] G. Camps-Valls, L. Gomez-Chova, J. Munoz-Mari, J. Vila-Frances, and J. Calpe-Maravilla, "Composite kernels for hyperspectral image classification," *IEEE Geosci. Remote Sens. Lett.*, vol. 3, no. 1, pp. 93–97, Jan. 2006.

[34] G. Camps-Valls, L. Gomez-Chova, J. Munoz-Mari, J. L. Rojo-Alvarez, and M. Martinez-Ramon, "Kernel-based framework for multitemporal and multisource remote sensing data classification and change detection," *IEEE Trans. Geosci. Remote Sens.*, vol. 46, no. 6, pp. 1822–1835, Jun. 2008.

[35] M. Fauvel, J. Chanussot, and J. A. Benediktsson, "Adaptive pixel neighborhood definition for the classification of hyperspectral images with Support Vector Machines and composite kernel," in *Proc. ICIP*, San Diego, CA, 2008, pp. 1884–1887.

[36] S. van der Linden, A. Janz, B. Waske, M. Eiden, and P. Hostert, "Classifying segmented hyperspectral data from a heterogeneous urban environment using support vector machines," *J. Appl. Remote Sens.*, vol. 1, no. 1, p. 013 543, Oct. 2007.

[37] Y. Tarabalka, J. Chanussot, J. A. Benediktsson, J. Angulo, and M. Fauvel, "Segmentation and classification of hyperspectral data using watershed," in *Proc. IGARSS*, Boston, MA, 2008, pp. III-652–III-655.

[38] *AVIRIS NW Indiana's Indian Pines 1992 Data Set*. [Online]. Available: ftp://ftp.ecn.purdue.edu/biehl/MultiSpec/92AV3C (original files) and ftp://ftp.ecn.purdue.edu/biehl/PC_MultiSpec/ThyFiles.zip (ground truth)

[39] J. A. Richards and X. Jia, *Remote Sensing Digital Image Analysis: An Introduction*. New York: Springer-Verlag, 1999.

[40] A. A. Green, M. Berman, P. Switzer, and M. D. Craig, "A transformation for ordering multispectral data in terms of image quality with implications for noise removal," *IEEE Trans. Geosci. Remote Sens.*, vol. 26, no. 1, pp. 65–74, Jan. 1988.

[41] A. Hyvärinen, J. Karhunen, and E. Oja, *Independent Component Analysis*. New York: Wiley, 2001.

[42] J. Wang and C.-I. Chang, "Independent component analysis-based dimensionality reduction with applications in hyperspectral image analysis," *IEEE Trans. Geosci. Remote Sens.*, vol. 44, no. 6, pp. 1586–1600, Jun. 2006.

[43] S. Moussaoui, H. Hauksdottir, F. Schmidt, C. Jutten, J. Chanussot, D. Brie, S. Douté, and J. A. Benediktsson, "On the decomposition of Mars hyperspectral data by ICA and Bayesian positive source separation," *Neurocomputing*, vol. 71, no. 10–12, pp. 2194–2208, Jun. 2008.

[44] E. Diday and J. C. Simon, "Clustering analysis," in *Digital Pattern Recognition*. Berlin, Germany: Springer-Verlag, 1976, pp. 47–94.

[45] G. Noyel, J. Angulo, and D. Jeulin, "Morphological segmentation of hyperspectral images," *Image Anal. Stereol.*, vol. 26, pp. 101–109, 2007.

[46] ITT Corporation, . For further information about the ENVI software. [Online]. Available: http://rsinc.com/envi/

[47] N. Kamagata, K. Hara, M. Mori, Y. Akamatsu, Y. Li, and Y. Hoshino, "A new method of vegetation mapping by object-based classification using high resolution satellite data," in *Proc. 1st Int. Conf. Object-Based Image Anal.*, 2006, vol. XXXVI-4/C42.

[48] S. C. Liew, C. W. Chang, and K. H. Lim, "Hyperspectral land cover classification of EO-1 Hyperion data by principal component analysis and pixel unmixing," in *Proc. IGARSS*, 2002, vol. 6, pp. 3111–3113.

[49] G. Celeux and G. Govaert, "A classification EM algorithm for clustering and two stochastic versions," *Comput. Stat. Data Anal.*, vol. 14, no. 3, pp. 315–332, Oct. 1992.

[50] X. R. Wang, S. Kumar, F. Ramos, and T. Kaupp, "Probabilistic classification of hyperspectral images by learning nonlinear dimensionality reduction mapping," in *Proc. Int. Conf. Inf. Fusion*, Jul. 2006, pp. 1–8.

[51] A. Martinez-Uso, F. Pla, J. M. Sotoca, and P. Garcia-Sevilla, "Clustering-based hyperspectral band selection using information measures," *IEEE Trans. Geosci. Remote Sens.*, vol. 45, no. 12, pp. 4158–4171, Dec. 2007.

[52] P. Masson and W. Pieczynski, "SEM algorithm and unsupervised segmentation of satellite images," *IEEE Trans. Geosci. Remote Sens.*, vol. 31, no. 3, pp. 618–633, May 1993.

[53] A. Solberg, T. Taxt, and A. Jain, "A Markov random field model for classification of multisource satellite imagery," *IEEE Trans. Geosci. Remote Sens.*, vol. 34, no. 1, pp. 100–113, Jan. 1996.

[54] S. Pal and P. Mitra, "Multispectral image segmentation using the rough-set-initialized EM algorithm," *IEEE Trans. Geosci. Remote Sens.*, vol. 40, no. 11, pp. 2495–2501, Nov. 2002.

[55] J. Driesen and P. Scheunders, "A multicomponent image segmentation framework," in *Proc. ACIVS*, 2008, pp. 589–600.

[56] S. Beaven, D. Stein, and L. Hoff, "Comparison of Gaussian mixture and linear mixture models for classification of hyperspectral data," in *Proc. IGARSS*, 2000, vol. 4, pp. 1597–1599.

[57] N. Acito, G. Corsini, and M. Diani, "An unsupervised algorithm for hyperspectral image segmentation based on the Gaussian mixture model," in *Proc. IGARSS*, Jul. 2003, vol. 6, pp. 3745–3747.

[58] L. Shapiro and G. Stockman, *Computer Vision*. Englewood Cliffs, NJ: Prentice-Hall, 2002.

[59] J.-O. Lapeyre and R. Strandh, "An efficient union-find algorithm for extracting the connected components of a large-sized image," Lab. Bordelais de Recherche en Inf., Bordeaux, France, Jan. 2004. Tech. Rep.

[60] K. Suzuki, I. Horiba, and N. Sugie, "Linear-time connected-component labeling based on sequential local operations," *Comput. Vis. Image Underst.*, vol. 89, no. 1, pp. 1–23, Jan. 2003.

[61] A. Widayati, B. Verbist, and A. Meijerink, "Application of combined pixel-based and spatial-based approaches for improved mixed vegetation classification using IKONOS," in *Proc. 23th Asian Conf. Remote Sens.*, 2002, pp. 1–8.

[62] G. Borgefors, "Distance transformations in digital images," *Comput. Vis. Graph. Image Process.*, vol. 34, no. 3, pp. 344–371, Jun. 1986.

[63] C. Chang and C. Linin *LIBSVM—A Library for Support Vector Machines*, 2008. [Online]. Available: http://www.csie.ntu.edu.tw/~cjlin/libsvm

[64] A. Plaza, J. A. Benediktsson, J. Boardman, J. Brazile, L. Bruzzone, G. Camps-Valls, J. Chanussot, M. Fauvel, P. Gamba, J. A. Gualtieri, M. Marconcini, J. C. Tilton, and G. Trianni, "Recent advances in techniques for hyperspectral image processing," *Remote Sens. Environ.,* in press. DOI: 10.1016/j.rse.2007.07.028.

[65] J. A. Benediktsson, J. A. Palmason, and J. R. Sveinsson, "Classification of hyperspectral data from urban areas based on extended morphological profiles," *IEEE Trans. Geosci. Remote Sens.*, vol. 43, no. 3, pp. 480–491, Mar. 2005.

[66] S. Aksoy, "Spatial techniques for image classification," in *Signal and Image Processing for Remote Sensing*, C. H. Chen, Ed. New York: Taylor & Francis, 2006, pp. 491–513.

[67] S. Tadjudin and D. Landgrebe, "Classification of high dimensional data with limited training samples," Ph.D. dissertation, School Elect. Comput. Eng., Purdue Univ., Hammond, IN, May 1998.

[68] N. Cristianini and J. Shawe-Taylor, *Support Vector Machines and Other Kernel-Based Learning Methods*. Cambridge, U.K.: Cambridge Univ. Press, 2000.

[69] H. P. Graf, E. Cosatto, L. Bottou, I. Dourdanovic, and V. Vapnik, "Parallel support vector machines: The cascade SVM," in *Advances in Neural Information Processing Systems*, vol. 17. Cambridge, MA: MIT Press, 2005.

[70] T. Habib, J. Inglada, G. Mercier, and J. Chanussot, "Speeding up support vector machine (SVM) image classification by a kernel series expansion," in *Proc. IEEE ICIP*, Oct. 2008, pp. 865–868.
[71] B. C. Catanzaro, N. Sundaram, and K. Keutzer, "Fast Support Vector Machine training and classification on graphics processors," EECS Dept., Univ. California, Berkeley, Berkeley, CA, Tech. Rep. UCB/EECS-2008-11, 2008.

Yuliya Tarabalka (S'08) received the B.S. degree in computer science from the Ternopil Ivan Pul'uj State Technical University, Ternopil, Ukraine, in 2005, and the M.Sc. degree in signal and image processing from the Grenoble Institute of Technology (INPG), Grenoble, France, in 2007. Since 2007, she has been working toward the Ph.D. degree, a cojoint degree between the University of Iceland, Reykjavik, Iceland, and INPG.

From July 2007 to January 2008, she was a Researcher with the Norwegian Defence Research Establishment, Norway. She is currently conducting her research at the Grenoble Images Speech Signals and Automatics Laboratory (GIPSA-Lab, INPG). Her current research work is funded by the "HYPER-I-NET" Marie Curie Research Training Network. Her research interests are in the areas of image processing, pattern recognition, hyperspectral imaging, and development of efficient algorithms.

Jón Atli Benediktsson (S'84–M'90–SM'99–F'04) received the Cand.Sci. degree in electrical engineering from the University of Iceland, Reykjavik, Iceland, in 1984, and the M.S.E.E. and Ph.D. degrees from Purdue University, West Lafayette, IN, in 1987 and 1990, respectively.

He is currently a Pro Rector for academic affairs and a Professor of electrical and computer engineering with the University of Iceland. He has held visiting positions with the Department of Information and Communication Technology, University of Trento, Trento, Italy, since 2002; the School of Computing and Information Systems, Kingston University, Kingston upon Thames, U.K., during 1999–2004; the Joint Research Centre of the European Commission, Ispra, Italy, in 1998; the Technical University of Denmark, Lyngby, Denmark, in 1998; and the School of Electrical and Computer Engineering, Purdue University, in 1995. In August 1997, he was a Fellow with the Australian Defence Force Academy, Canberra, A.C.T., Australia. From 1999 to 2004, he was the Chairman of the energy company Metan Ltd. He was also the Chairman of the University of Iceland's Science and Research Committee from 1999 to 2005. Since 2006, he has been the Chairman of the University of Iceland's Quality Assurance Committee. He coedited (with Prof. D. A. Landgrebe) a Special Issue on Data Fusion of TGARS (May 1999) and (with P. Gamba and G. G. Wilkinson) a Special Issue on Urban Remote Sensing from Satellite (October 2003). His research interests include remote sensing, pattern recognition, neural networks, image processing, and signal processing, and he has published extensively in those fields.

Dr. Benediktsson was the Past Editor and is currently an Associate Editor for the IEEE TRANSACTIONS ON GEOSCIENCE AND REMOTE SENSING (TGARS) and an Associate Editor for the IEEE GEOSCIENCE AND REMOTE SENSING LETTERS. From 1999 to 2002, prior to being Editor, he was an Associate Editor for TGARS. From 1996 to 1999, he was the Chairman of GRSS Technical Committee on Data Fusion and was elected to the Administrative Committee of the GRSS for the terms 2000–2002 and 2008–2010. In 2002, he was appointed as Vice President of Technical Activities of GRSS, and in 2008, he was appointed as Vice President of Professional Activities of GRSS. He was the founding Chairman of the IEEE Iceland Section and served as its Chairman from 2000 to 2003. He was a member of a NATO Advisory Panel of the Physical and Engineering Science and Technology Subprogram (2002–2003). He was a member of Iceland's Science and Technology Council (2003–2006) and a member of the Nordic Research Policy Council (2004). He received the Stevan J. Kristof Award from Purdue University, in 1991, as an outstanding graduate student in remote sensing. In 1997, he was the recipient of the Icelandic Research Council's Outstanding Young Researcher Award. In 2000, he was granted the IEEE Third Millennium Medal. In 2004, he was a corecipient of the University of Iceland's Technology Innovation Award. In 2006, he received the yearly research award from the Engineering Research Institute, University of Iceland. In 2007, he received the Outstanding Service Award from the IEEE Geoscience and Remote Sensing Society. He is a member of Societas Scinetiarum Islandica and Tau Beta Pi.

Jocelyn Chanussot (M'04–SM'04) received the M.Sc. degree in electrical engineering from the Grenoble Institute of Technology (INPG), Grenoble, France, in 1995, and the Ph.D. degree from Savoie University, Annecy, France, in 1998.

In 1999, he was with the Geography Imagery Perception Laboratory for the Delegation Generale de l Armement (DGA-French National Defense Department). Since 1999, he has been with INPG, where he was an Assistant Professor from 1999 to 2005, an Associate Professor from 2005 to 2007, and is currently a Professor of signal and image processing. He is currently conducting his research at the Grenoble Images Speech Signals and Automatics Laboratory (GIPSA-Lab, INPG). His research interests include image analysis, multicomponent image processing, nonlinear filtering, and data fusion in remote sensing.

Dr. Chanussot is the founding President of IEEE Geoscience and Remote Sensing French chapter (2007) and a member of the IEEE Geoscience and Remote Sensing AdCom (2009–2011). He is the General Chair of the first IEEE GRSS Workshop on Hyperspectral Image and Signal Processing, Evolution in Remote sensing (WHISPERS). He was the Cochair of the GRS Data Fusion Technical Committee (2005–2008) and a member of the Machine Learning for Signal Processing Technical Committee of the IEEE Signal Processing Society (2006–2008). He was an Associate Editor for the IEEE GEOSCIENCE AND REMOTE SENSING LETTERS (2005–2007) and for *Pattern Recognition* (2006–2008). He is an Associate Editor for the IEEE TRANSACTIONS ON GEOSCIENCE AND REMOTE SENSING.